

Gate voltage control of the $AlO_x/SrTiO_3$ interface electrical properties

J. Delahaye and T. Grenet

Institut Néel, CNRS & Université Grenoble Alpes, F-38042 Grenoble, France

E-mail: julien.delahaye@neel.cnrs.fr

Abstract. Electron-beam deposition of an insulating granular aluminium or of an off-stoichiometric amorphous alumina layer on a $SrTiO_3$ surface is a simple way to get a metallic interface from insulating materials. No heating nor specific preparation of the $SrTiO_3$ surface are needed. In this paper, we investigate how the electrical properties of this interface can be tuned by the use of a back gate voltage (electrical field through the $SrTiO_3$ substrate). We demonstrate that the slow field-effect observed at room temperature can be used to tune reversibly and in a controlled way the low temperature electrical properties of the interface. In particular, important parameters of a transistor such as the amplitude of the resistance response to gate voltage changes or the existence of an “on” or an “off” state at zero gate voltage and at low temperature can be adjusted in a single sample. This method should be applicable to any $SrTiO_3$ -based interface in which oxygen vacancies are involved and might provide a powerful way to study the metal or superconductor insulator transition observed in such systems.

PACS numbers: 72.20.-i 71.30.+h

1. Introduction

Various techniques have been successfully used through the last 50 years to put insulating SrTiO_3 (STO) crystals into a metallic state. With standard chemical doping and high temperature annealing under vacuum [1, 2], the metallic state extends over the bulk of the crystal. With ion-milling [3–7], UV exposure [8, 9], UHV cleaving [10] and oxide layer deposition [11–16], the metallic state can be confined close to the STO surface ‡. The oxide layer deposition technique was first restricted to the epitaxial growth of oxides by pulsed laser deposition at high temperature, the most famous example being the $\text{LaAlO}_3/\text{SrTiO}_3$ (LAO/STO) heterostructure [12, 13, 17, 18]. But surface metallic states were also recently observed by using pulsed laser [19–22] and e-beam [23] depositions of amorphous oxides at room temperature. The respective roles of oxides non stoichiometry (oxygen, cations), adsorbates, ions inter-diffusion and electronic reconstruction in the formation of this surface metallic state remain an active and controversial issue [11, 13, 17, 20, 24–34].

In this article, we report on electrical field effect measurements of STO crystals, on which an insulating granular aluminum or an oxygen deficient alumina layer (thereafter referred to as the AlO_x layer) was deposited at room temperature by electron gun evaporation. We have demonstrated recently that such deposition can put the STO surface into a metallic state [23]. The simplicity of the manufacturing process (no heating, no surface preparation) makes this method very attractive compared to the more sophisticated techniques currently used. The most likely origin of this metallic state is the formation of oxygen vacancies in the STO substrate close to the AlO_x/STO interface, the oxygen being “pumped off” from STO when the AlO_x layer is deposited on top [23]. Oxygen vacancies in STO are known to release electrons for the conduction and can lead to a metallic state if their concentration is large enough. The exact thickness of this metallic state is not known but its electrical parameters (charge carrier surface density and mobility, sheet resistance value and temperature dependence, etc.) are very similar to the 2D electron gas obtained by the pulsed laser deposition of oxides, which strongly suggests that it is confined close to the interface [23].

When STO crystals are doped in the bulk by chemical impurities or oxygen vacancies, the metal-insulator transition occurs at small charge carrier densities compared to other oxides or even standard doped semi-conductors. The 3D critical charge density which corresponds to the metal-insulator transition is not precisely known but metallic states are reported for impurity densities as low as 10^{16}cm^{-3} [2]. The high value of the STO dielectric constant, especially at low temperature, may explain this striking property. At 2D, a metallic-like behaviour is observed for surface charge densities as low as a few 10^{13}cm^{-2} [35]. Such a value corresponds to the surface charge density that can be added or removed in a standard field effect experiment, where a gate voltage is applied between the STO surface and a metallic gate over an insulating

‡ Note that if the thickness of the metallic layer can be of less than 10nm for oxide heterostructures, it is much larger (about 100nm or even more) for ion-milled surfaces.

material (the gate insulator). STO is thus a system in which large modulations of the electrical resistance are expected upon the application of a gate voltage [36].

A large number of electrical field effect experiments have been performed on STO crystal based devices. Many different situations were explored: the STO surface was in the “on” (metallic or superconducting) state or in the “off” (insulating) state when no gate voltage was applied, the bulk of the STO crystal was used as the gate insulator (“back gate” geometry) or another insulating material was deposited on top (“top gate” geometry), the temperature of the measurement was 300K or much lower (4K), etc. The observed resistance response to gate voltage changes are also quite various: they can be fast or slow, small or with relative changes of many orders of magnitude, associated with memory effects and hysteresis, etc. [5, 13, 35, 37–61]. But in all these studies, the electrical properties of the interface are determined by the fabrication parameters. What we show in this article is that the low temperature electrical properties of our AlO_x/STO interface can also be changed after its making.

We studied the field effect in AlO_x/STO interfaces in the “back gate” geometry from room T to 4K. Our main results can be summarized as follows. At room temperature, the response to the application of a non-zero gate voltage (V_g) is dominated by slow changes of the resistance, which can increase by three orders of magnitude the resistance of a metallic-like interface. Since this slow resistance response is reversible and practically frozen below $\simeq 250\text{K}$, it can be used to tune the electronic state (metallic or insulating) of a given starting metallic-like interface, and to stabilize a large range of low temperature properties. For example, a state showing a huge field effect at 4K could be obtained (resistance changing by 6 orders of magnitude with a gate field of 0.6kV/cm). The respective roles of oxygen vacancies electro-migration and standard charge injection processes will be discussed.

2. Elaboration and measurement techniques

The samples were made according to Ref. [23]. STO crystals one side polished, (100) oriented and 0.5mm thick were purchased from Neyco company. The polished surface was simply cleaned by successive ultrasonic bath in trichloroethylene, acetone and alcohol before being mounted in an electron beam evaporator. Al contacts, 20nm thick, were deposited first. Then, 40nm of insulating granular Al or 5nm of O_2 deficient alumina passivated by 95nm of stoichiometric alumina was deposited between the Al contacts without breaking the vacuum. The O_2 deficient alumina layer was obtained by the evaporation of alumina at 0.5\AA/s under an O_2 pressure of less than 10^{-5}mbar , the stoichiometric alumina layer by the evaporation of alumina at 0.5\AA/s under an O_2 pressure of $2 \times 10^{-4}\text{mbar}$ and the insulating granular Al layer by the evaporation of pure Al at 1.8\AA/s under an O_2 pressure of $4 - 5 \times 10^{-5}\text{mbar}$. The base pressure of the evaporator is less than 10^{-6}mbar . As long as the sheet resistances of the samples are the same, we did not observe any significant difference between the field effect response of granular Al and O_2 deficient alumina / STO interfaces.

The active channel between the Al contacts (i.e. the part of the surface covered by the AlO_x overlayer) has a typical size of $1\text{mm} \times 2\text{mm}$. Its electrical resistance was measured in a two contact MOSFET-like configuration § and unless otherwise specified, in the ohmic regime (linear part of the $I - V_b$ curves, V_b being the bias voltage). Depending on the resistance value, either current bias or voltage bias were used. In our electrical field effect measurements, the gate insulator is the STO substrate itself and no leakage currents were detected with the V_g values used (leakage currents below 1pA , maximum absolute V_g value of 100V corresponding to an electric field of 2kV/cm). The bias voltage V_b was usually kept much smaller than V_g in order to avoid any mix up between the two parameters. The gate contact was made on the unpolished side of STO crystal with silver paint and its polarity is such that it is connected to the plus terminal of the V_g source (see Figure 1).

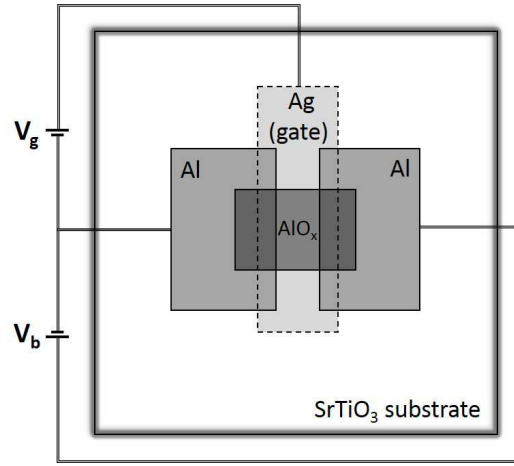


Figure 1. Sketch of a typical sample: the STO substrate is $10 \times 10 \times 0.5\text{mm}$, the Al contacts $4 \times 2.5\text{mm}$, the active AlO_x channel (the part between the Al contacts) $\simeq 2 \times 1\text{mm}$ and the gate width (on the other side of the STO substrate) is $\simeq 2\text{mm}$. The polarities of the gate (V_g) and bias (V_b) voltages are also indicated.

3. Room temperature modulation of the resistance

Depending on the oxygen pressure (Al/O ratio during the evaporation), we can get samples with room temperature R_s values from $\simeq 20\text{k}\Omega$ to unmeasurably large values [23]. Typical $R_s - T$ curves of low and high- R_s samples are plotted on Figure 2 in the range $4\text{K} - 300\text{K}$. The resistance of a $R_{s300\text{K}} = 30\text{k}\Omega$ sample decreases by a factor of 10 between 300K and 30K , with a small resistance increase at lower temperature as observed elsewhere for samples with similar R_s values [27, 48]. The resistance of a $R_{s300\text{K}} = 500\text{M}\Omega$ sample displays instead a fast increase (close to an exponential) when the temperature is lowered and is already not measurable (R above $100\text{G}\Omega$) around

§ For metallic samples, two and four contacts configurations could be used and no significant difference was observed.

150K. The transition from a room temperature metallic-like (temperature coefficient dR/dT positive around 300K ||) to a room temperature insulating-like (dR/dT negative around 300K) behaviour occurs around $R_{s300K} \simeq 1M\Omega$. We will focus thereafter on metallic-like interfaces, having R_s values in the range 20 – 30k Ω at 300K. A resistance increase of $\simeq 10\%$ which saturates within about 2 hours is observed when the samples are transferred from ambient daylight to darkness, and all the following measurements were thus performed after at least one day in the dark.

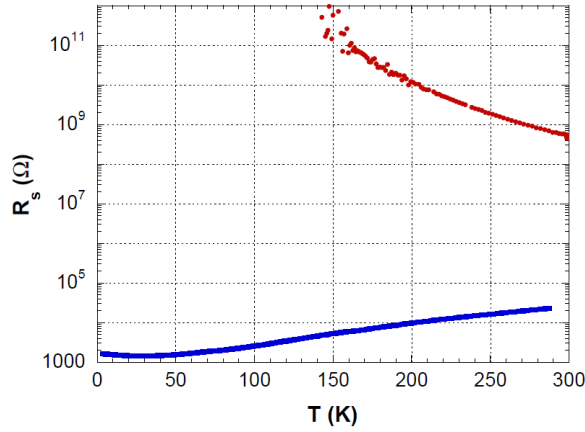


Figure 2. R_s versus T between 4K and 300K for two “extreme” AlO_x/STO samples. The high- R_s sample was kept 3 days in the dark before the measurement. The highest resistance measurable in our experimental set-up is of $10^{10} - 10^{11}\Omega$.

Typical behaviours of such low R_s samples submitted to repeated gate voltage cycles ($V_g = 0V, +30V, 0V, -30V$) are plotted in Figure 3. Such V_g cycles are commonly used in STO-based field effect measurements in order to quantify fast and slow responses to V_g changes and to reveal a potential memory of the V_g values experienced by the sample. Apart from small fast (faster than $\simeq 1s$) R_s changes occurring when V_g is switched, the R_s response is found to be dominated by slow variations. Each stay $\simeq 1000s$ long under a positive V_g results in a slow resistance decrease with the opposite trend under a negative V_g . Moreover, during the 0V stay, the resistance keeps a memory of the latest V_g experienced by the sample: when V_g is switched back to 0V, the resistance tends to come back to its value before the latest V_g change. But these drifts are much slower than under positive or negative V_g and the R_s restoration is only partial. The R_s values observed over one V_g cycle are therefore not symmetrical to the initial 0V value. R_s modulations are reproducible over many gate voltage cycles and typical values of slow and fast resistance variations are indicated in the legend of Figure 3. Interestingly enough, the resistance modulations are strongly reduced when the samples are exposed to daylight (see Supplementary materials A).

Much larger R_s changes are obtained when non-zero V_g are applied over longer

|| Such samples are not metallic in the strict sense since most of them display a clear diverging resistance at low temperature.

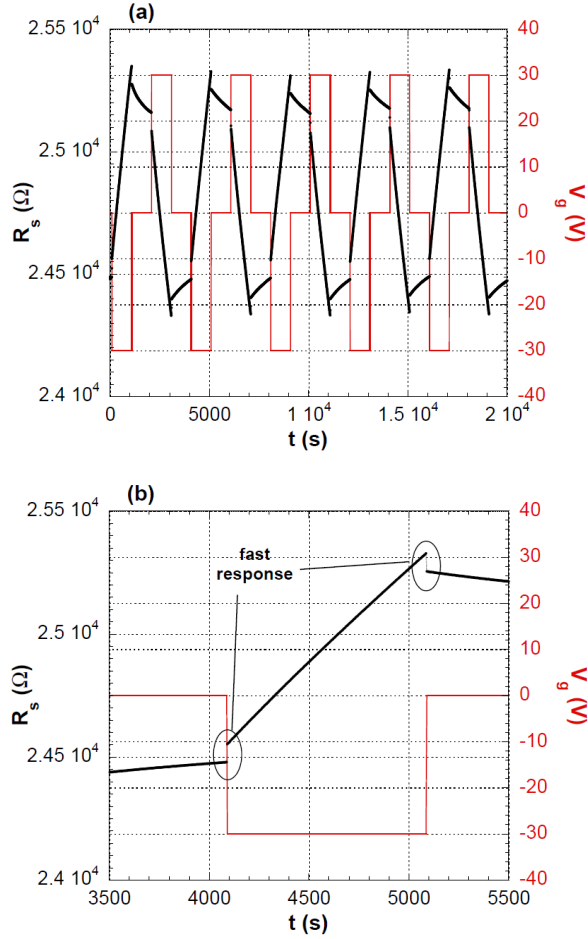


Figure 3. (a) R_s as a function of time under repeated V_g cycles 0V, -30V, 0V, 30V at room temperature. (b) Zoom of the top figure over a reduced time scale. The slow R_s drift is about 3% over 1000s while the fast shifts corresponding to a V_g change of $\pm 30\text{V}$ are equal to 0.33%.

times. Starting from a “fresh” (no V_g history) low- R_s sample ($R_s = R_{sref} = 30\text{k}\Omega$), R_s reaches a minimum value about 10% smaller after few hours under $V_g = 30\text{V}$, while a steady R_s increase is observed over 20h under $V_g = -30\text{V}$, up to a maximum value of $\simeq 10\text{M}\Omega$ (see Figure 4). Such a value is already beyond the metallic-like to insulating crossover of $\simeq 1\text{M}\Omega$ discussed before.

The fast field-effect can be simply understood as a standard V_g induced charge injection or removal in the system. The fact that a V_g increase is associated with a resistance drop, and a V_g decrease with a resistance jump is in qualitative agreement with the negative sign of the charge carriers obtained by Hall effect measurements [23]. We can go one step further and use the amplitude of the resistance jumps or drops to estimate the surface charge carrier density n_s at the interface. If all the charge carriers involved in the conduction have the same mobility μ , the relative amplitudes of resistance

μ The charge carrier mobilities were found to be in the range $1 - 10\text{cm}^2.\text{V}^{-1}.\text{s}^{-1}$ for surface and bulk metallic-like states [2, 27]. This approximation should thus be reasonable at least for low- R_s

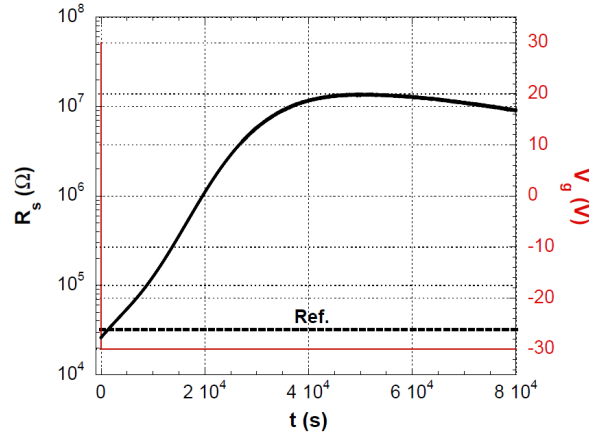


Figure 4. R_s response following a V_g change from 30V to -30V after the samples have been allowed to reach their minimum resistance values under $V_g = 30\text{V}$. The R_s values before any V_g change are indicated by the dotted lines.

jumps or drops $|\Delta R_s/R_s|$ should be equal to the relative changes in the surface charge carrier density $|\Delta n_s/n_s|$ (as long as the relative changes are smaller than 1). Assuming a simple plane-plane capacitance geometry, $\Delta n_s(\Delta V_g) = (\epsilon/d)\Delta V_g$ where ϵ is the dielectric constant of the STO substrate ($300\epsilon_0$ at 300K) and d its thickness (0.5mm). For the sample of Figure 3 ($R_s = 25\text{k}\Omega$), $\Delta R_s(30\text{V})/R_s$ and thus $\Delta n_s(V_g)/n_s$ are equal to 0.3% . A V_g change of 30V corresponds at 300K to $\Delta n_s(30\text{V}) = 1.0 \times 10^{11}\text{e}/\text{cm}^2$, which gives a n_s estimate of $3 \times 10^{13}\text{e}/\text{cm}^2$. This n_s value is in quantitative agreement with Hall effect measurements on samples of similar R_s [23].

Let's now discuss the prominent slow part of the field effect. In our samples, the charge carriers are supposed to be electrons released by oxygen vacancies in the STO substrate. When $V_g \neq 0$, an electrical field exists in the bulk of the STO substrate up to the AlO_x/STO interface conducting state. Note that this external field adds to a possible internal field present at the interface when $V_g = 0$. According to different experiments, oxygen vacancies have a significant mobility in STO at room temperature [7, 54, 62]. It is thus tempting to explain the slow R_s changes observed under non-zero V_g as slow drifts of the oxygen vacancies under this electric field. If $V_g < 0$ (resp. > 0), the electrical field is such that it pulls (resp. pushes) the positively charged oxygen vacancies further from (resp. closer to) the interface. The concentration of oxygen vacancies close to the AlO_x/STO interface thus decreases (resp. increases) under negative (resp. positive) V_g . By analogy with what occurs in disordered induced metal-insulator transition, the decrease of the charge carrier concentration is accompanied by a strong suppression of their mobility below some critical concentration [63]. The crucial role of mobility changes is supported by a quantitative analysis on the sample of figure 4: its surface charge carrier density (deduced from fast resistance jumps and drops, see before) is divided by only 7 between the minimum and maximum R_s states while R_s is multiplied

by 400⁺. When V_g is switched back to 0V, the V_g induced electro-migration stops and the resistance shifts are strongly reduced, giving rise to the memory effect described before.

Slow resistance drifts and memory effects are indeed quite common at room temperature in STO-based field effect devices [13, 35, 54]. They are usually attributed to the electro-migration of oxygen vacancies in the STO substrate, an hypothesis which is strengthened by the fact that these features are smaller or absent when top gated insulators are used [35, 53, 55, 56]. But our explanation based on a strong concentration dependence of the charge carriers mobility doesn't seem to be universal: in amorphous LAO/STO heterostructures, the large and slow R_s changes are accompanied by large changes of the surface charge density, with only a negligible alteration of the mobility [54].

In order to test in more detail the oxygen vacancy electro-migration hypothesis, we have studied how the slow R_s drifts were affected by temperature changes around 300K. Our protocol was the following. The sample was first let to equilibrate under 30V until R_s reached its minimum value. Then, V_g was changed to -30V and the subsequent R_s increase was measured as a function of time. The same protocol was repeated at different temperatures between 10°C and 50°C. Typical results are plotted in Figure 5. It is clearly seen that the R_s changes are strongly slowed down when T is reduced. Moreover, all the curves can be merged together far from the saturation regime by normalizing R_s to its value at 30V and the time scale by an ad-hoc characteristic time for each T (see the legend of Figure 6 for the exact definition of this characteristic time). Even if the T range is small in kelvin scale, the T dependence of the characteristic times is close to an activated behavior (see Figure 6), with an activation energy of 0.7eV *. A similar value was found in a much more resistive sample, having $R_{s300K} = 800M\Omega$. This value of 0.7eV is in agreement with previous experimental and theoretical estimates for oxygen vacancy diffusion coefficient in STO [62, 64, 65], which strengthens our hypothesis that the electro-migration of oxygen vacancies (isolated or as clusters) is responsible of the slow resistance drifts observed under $V_g \neq 0$. In amorphous LAO/STO interfaces [54], no quantitative estimate of the activation energy was done, but the resistance drifts are absent below $\simeq 270K$, in qualitative agreement with the strong temperature dependence highlighted in Figures 5 and 6.

4. V_g tuned interfaces measured at low temperature

We are now going to demonstrate how this strong temperature dependence of the slow field effect can be used to tune the low temperature properties of a unique AlO_x/STO

⁺ The fact that the resistance goes through a maximum under negative V_g in low- R_s samples cannot be understood within this simplified picture. It might result from the combined effects of an internal electrical field at the AlO_x/STO interface and of a charge mobility dependence with the distance to the interface.

* The exact definition of the characteristic times will change the time scale in Figure 6 but not the activation energy extracted.

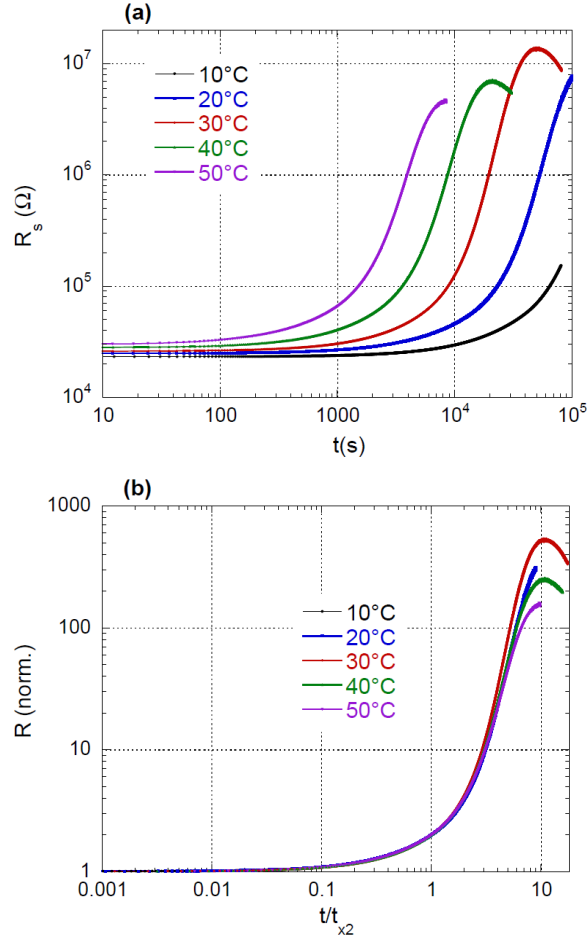


Figure 5. (a) R_s response to a V_g change from 30V to -30 V and for different T between 10°C and 50°C (see the text for details). (b) R_s normalized to the 30V reference value plotted as a function of $t/t_{\times 2}$ where $t_{\times 2}$ is the time at which R_s has been multiplied by 2 at a given T .

interface. The protocol is as follows. Starting with a metallic-like sample having $R_{s300K} = 20 - 30k\Omega$, we first apply a negative V_g of -30 V until the desired R_s value is obtained (values up to $10M\Omega$ can be achieved, see before). Then, we quickly cool down the sample below $\simeq 250K$, usually under $V_g = 0$ V, in order to freeze the sample parameters. At this temperature, the characteristic time of the slow resistance drifts are already so long that they cannot be measured in practice. Typical $R_s - T$ curves of such V_g -tuned sample are plotted in Figure 7. It is seen that, like in non V_g -tuned samples, the $R_s - T$ behavior can indeed be changed from metallic-like ($dR_s/dT > 0$ around 300K) to insulating-like ($dR_s/dT < 0$ around 300K) when R_s at 300K exceeds $\simeq 1M\Omega$. A large R_s range from a few $k\Omega$ to non measurable resistances ($R_s > 10G\Omega$) can be obtained at 4K. The low T differences observed between cool-down and warm-up curves are due to the irreversible resistance increase which occurs during the first V_g cycles at low T (see Supplementary materials B).

The typical 4K response of a non V_g -tuned sample ($R_{s300K} = 30k\Omega$) to repeated V_g

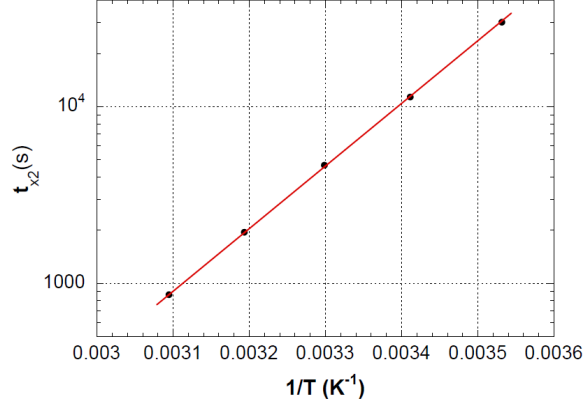


Figure 6. Characteristic times $t_{\times 2}$ extracted from the scaling analysis of $R_s(t, V_g, T)$ data (see Figure 5). The straight line corresponds to an activated behaviour $t_{\times 2} = A \exp(-T_0/T)$, with $T_0 = 8100\text{K}$.

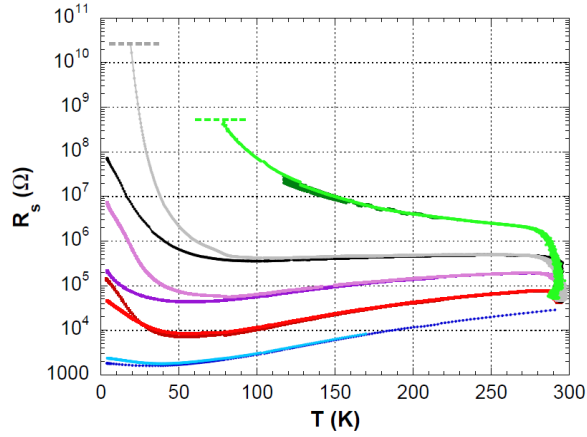


Figure 7. $R_s - T$ curves measured on a low- R_s sample after successive V_g modulations of its resistance at 300K (see the text for details). Dark and light colors are used respectively for the cool-down and the warm up of the sample (after V_g cycles at 4K). All the curves were measured under $V_g = 0\text{V}$ except the dark red one which corresponds to a cool down under -30V . The near vertical parts of the curves observed around room temperature reflect the stays under -30V which are performed prior to the cool-down in order to adjust the R_s value of the sample, and the slow recovery of the initial R_s value under 0V when the sample is warmed up to room temperature.

cycles (0V , $-V_{g0}$, 0V , V_{g0}) is plotted on Figure 8. The fast field effect now dominates the R_s modulation and is much larger than at 300K for the same sample: R_s is multiplied by more than 2 after a V_g change from 0V to -50V , compared to an increase of less than 1% at 300K . A memory effect is also present, i.e. the R_s value at $V_g = 0\text{V}$ depends of the previous V_g applied.

But when V_g tuned samples having larger R_s values are measured, the electrical field effects change dramatically. The relative R_s difference is about 50% between $V_g = -30\text{V}$ and 30V at 4K when $R_{s300\text{K}} = 30\text{k}\Omega$ (non V_g tuned sample) and it becomes as large as 6

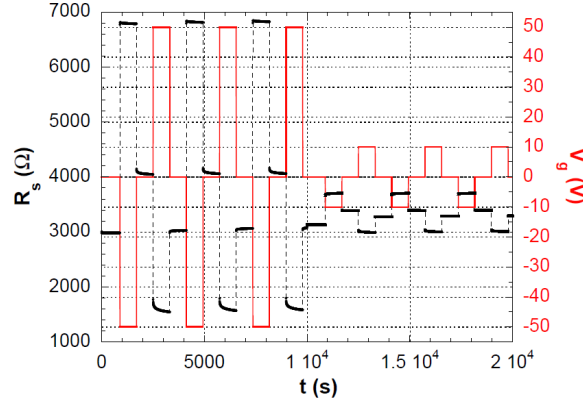


Figure 8. R_s versus time during 50V and 10V V_g cycles at 4K for a low- R_s sample ($R_{s300K} = 30k\Omega$).

orders of magnitude when $R_{s300K} = 60k\Omega$ following V_g tuning (see Figure 9). When R_s is further increased, the resistance of the interface becomes unmeasurable under $V_g = 0V$ (transistor in the “off” state, $R_s > 10G\Omega$) and is as low as $10k\Omega$ under $V_g = 50V$. Moreover and like in non V_g tuned samples, the large R_s modulations observed at 4K are accompanied by memory effects at $V_g = 0V$, which take the form of an hysteresis in the $R_s - V_g$ curves of Figure 10. Note that when R_s increases, the $R_s - V_g$ values become also strongly bias dependent.

Like at room temperature, the amplitude of the instantaneous field effect in non V_g tuned low- R_s samples is compatible with a standard charge injection process by the gate. According to our Hall effect measurements on a low- R_s sample, we know that the surface charge density n_s is almost constant with the temperature between 4K and 300K \ddagger . But the dielectric constant of STO has a strong temperature dependence: ϵ_r is around 300 at 300K, 2000 at 77K, 20000 at 4K (under a small electric field) [66, 67] and 10000 for $V_g = 50V$ (electrical field of $1kV/cm$) [66]. We thus expect the surface charge densities induced by the gate voltage $\Delta n_s(V_g)$ to be about ten times larger at 77K and 100 times larger at 4K than at 300K (at small enough V_g). It corresponds roughly to what is indeed measured for the low- R_s sample of Figure 8 when $\Delta R_s/R_s$ is small: $\Delta R_s/R_s(50V) = 0.5\%$ at 300K, $\Delta R_s/R_s(50V) = 6\%$ at 77K and $\Delta R_s/R_s(5V) = 5\%$ at 4K. The fact that the R_s modulation becomes larger in relative value in samples having increasing R_s values can simply be explained by a decrease of their surface charge densities.

As for V_g tuned high- R_s samples, large resistance modulations at low temperatures have been reported in many studies on STO-based field effect devices in the back gate configuration [5, 46, 48]. Beyond the effect of a n_s change, the mobility was also found to play a major role in the resistance modulations [5, 48, 60]. Under $V_g < 0$, the electron gas is compressed closer to the interface and the mobility is lowered, while under $V_g > 0$,

\ddagger For a sample having $R_s = 100k\Omega$ at 300K, n_s was found to increase from $2 \times 10^{13}e/cm^2$ at 300K up to $2.4 \times 10^{13}e/cm^2$ at 80K, before decreasing down to $1.6 \times 10^{13}e/cm^2$ at 4K.

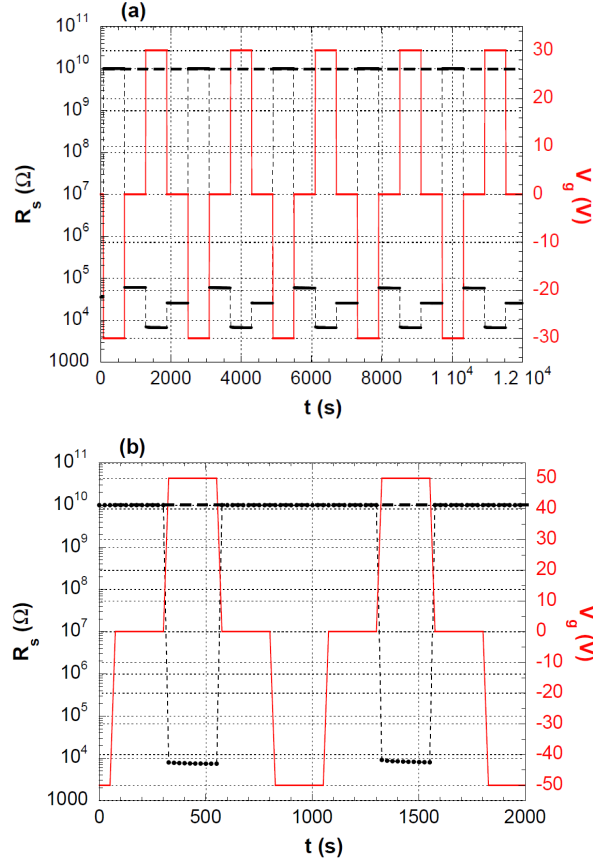


Figure 9. (a) R_s response to V_g cycles at 4K for a low- R_s sample V_g tuned at room T ($R_{s300K} = 60k\Omega$, bias voltage 10mV). R_s is immeasurably large (above $10G\Omega$) under $-30V$ and of only $7k\Omega$ under $30V$. (b) R_s versus V_g at 4K for the same low- R_s sample V_g tuned to $R_{s300K} = 120k\Omega$. R_s is measurable only under $V_g = 50V$.

the electron gas is extended towards the STO volume and the mobility is enhanced. The complete understanding of gating effects also requires the inclusion of the permittivity nonlinearities with the electric field [48].

The origin of the memory effect and the hysteresis observed in Figures 8 and 9 remains unclear. Dielectric studies have shown that a ferroelectric state can be induced by a strong enough electrical field in STO crystals, due to the proximity of the ferroelectric transition [67]. This ferroelectric state was usually found to be suppressed when T is increased beyond 50 – 100K. Hysteresis and remnant polarization were measured at $1kV/cm$ in Ref. [68, 69], but also under smaller fields in LAO/STO interfaces [46, 48, 70]. In Ref. [70], the resistance hysteresis was found to be related to a field induced polar order localized in the STO substrate about $1\mu m$ below the LAO/STO interface [70]. Interestingly enough, small or no hysteresis was found at low T in field effect measurements in top-gate configuration [55], indicating that the STO substrate plays the dominant role in the effect. In our case, a memory effect is visible at 4K already at $0.2kV/cm$ but not at 77K up to $1kV/cm$.

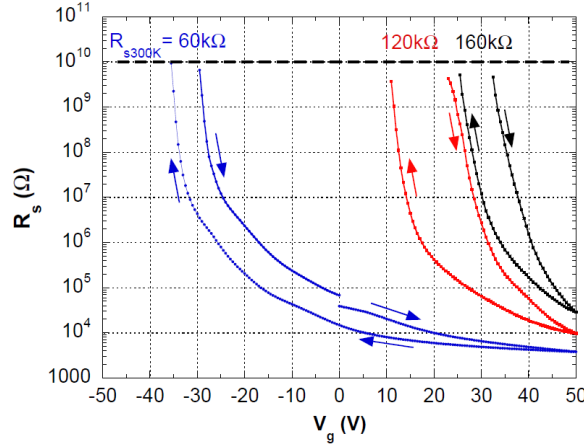


Figure 10. R_s versus V_g at 4K for the sample already measured in Figure 9 and V_g tuned at room temperature to three different R_{s300K} values: 60k Ω , 120k Ω and 160k Ω . V_g was continuously swept from 0V to 50V, then to -50V and then back to 0V and the bias voltage was fixed to 100mV. The curves are not plotted when R_s exceeds the highest measurable value of our set-up (dotted line), which restrains the plotted curves to positive V_g values for the two most resistive ones.

5. Conclusion

Our results show how the electrical properties of a metallic-like AlO_x/STO interface can be tuned by the use of a back-gate voltage V_g . At room temperature, a slow increase of the resistance is observed under a negative V_g . This resistance increase can be large (many orders of magnitude) if V_g is applied for a long enough time and the initial resistance value can be restored with the use of a positive V_g . The sample sheet resistance R_s can thus be tuned on a controlled and reversible way to any value spanning from a metallic-like ($R_s = 20\text{k}\Omega$, $dR/dT > 0$ at 300K) to an insulating-like behavior ($R_s > 1\text{M}\Omega$, $dR/dT < 0$ at 300K). The activation energy of these slow resistance change time scales is about 0.7eV which strongly suggests that they are related to oxygen vacancy electro-migration. By pulling the oxygen vacancies in the volume of the STO crystal (the gate insulator material), the electrical field reduces the charge carriers density and mobility.

If the interface resistance is V_g tuned at room temperature and then rapidly cooled down below 250K, a large set of stable interface electrical properties can be obtained. Such process can be used for example to increase the field effect amplitude at 4K: fast resistance changes as large as six orders of magnitude can thus be obtained under V_g cycles. We believe that this V_g tuning technique at room temperature should also be applicable to the other 2D STO-based metallic systems where similar slow field effects have been reported. Beyond the adjustment of low temperature transistors parameters, it should allow the fine study of the metal-insulator transition or even the transition to the superconducting state as a function of the interface parameters (charge carriers density and mobility) in a single sample.

- [1] Frederikse H P, Thurber W R and Hosler W R 1964 *Physical Review* **134** 442
- [2] Spinelli A, Torija M A, Liu C, Jan C and Leighton C 2010 *Physical Review B* **81** 155110
- [3] Reagor D W and Butko V Y 2005 *Nature Materials* **4** 593
- [4] Kan D, Terashima T, Kanda R, Masuno A, Tanaka K, Chu S, Kan H, Ishizumi A, Kanemitsu Y, Shimakawa Y *et al.* 2005 *Nature Materials* **4** 816
- [5] Ngai J, Segal Y, Su D, Zhu Y, Walker F, Ismail-Beigi S, Le Hur K and Ahn C 2010 *Physical Review B* **81** 241307
- [6] Herranz G, Copie O, Gentils A, Tafrá E, Basletić M, Fortuna F, Bouzehouane K, Fusil S, Jacquet É, Carrétéro C *et al.* 2010 *Journal of Applied Physics* **107** 103704
- [7] Gross H, Bansal N, Kim Y S and Oh S 2011 *Journal of Applied Physics* **110** 073704
- [8] Kozuka Y, Hikita Y, Susaki T and Hwang H 2007 *Physical Review B* **76** 085129
- [9] Meevasana W, King P, He R, Mo S, Hashimoto M, Tamai A, Songsiriritthigul P, Baumberger F and Shen Z 2011 *Nature Materials* **10** 114
- [10] Santander-Syro A, Copie O, Kondo T, Fortuna F, Pailhes S, Weht R, Qiu X, Bertran F, Nicolaou A, Taleb-Ibrahimi A *et al.* 2011 *Nature* **469** 189
- [11] Chen Y, Bovet N, Trier F, Christensen D, Qu F, Andersen N H, Kasama T, Zhang W, Giraud R, Dufouleur J *et al.* 2013 *Nature Communications* **4** 1371
- [12] Carretero C 2010 *Hétérostructures d'oxydes de structure pérovskite : propriétés structurales et électroniques de l'interface $\text{LaAlO}_3/\text{SrTiO}_3$* Ph.D. thesis Université Pierre et Marie Curie
- [13] Thiel S 2009 *Study of Interface Properties in $\text{LaAlO}_3/\text{SrTiO}_3$ Heterostructures* Ph.D. thesis Universität Augsburg
- [14] Basletic M, Maurice J L, Carrétéro C, Herranz G, Copie O, Bibes M, Jacquet É, Bouzehouane K, Fusil S and Barthélémy A 2008 *Nature Materials* **7** 621
- [15] Sing M, Berner G, Goß K, Müller A, Ruff A, Wetscherek A, Thiel S, Mannhart J, Pauli S, Schneider C *et al.* 2009 *Physical Review Letters* **102** 176805
- [16] Reyren N, Thiel S, Caviglia A, Kourkoutis L F, Hammerl G, Richter C, Schneider C, Kopp T, Rüetschi A S, Jaccard D *et al.* 2007 *Science* **317** 1196
- [17] Ohtomo A and Hwang H 2004 *Nature* **427** 423
- [18] Huijben 2006 *Interface Engineering for Oxide Electronics: Tuning electronic properties by atomically controlled growth* Ph.D. thesis University of Twente
- [19] Chen Y, Pryds N, Kleibeuker J E, Koster G, Sun J, Stamate E, Shen B, Rijnders G and Linderoth S 2011 *Nano Letters* **11** 3774
- [20] Liu Z, Li C, Lü W, Huang X, Huang Z, Zeng S, Qiu X, Huang L, Annadi A, Chen J *et al.* 2013 *Physical Review X* **3** 021010
- [21] Fuchs D, Schäfer R, Sleem A, Schneider R, Thelen R and von Löhneysen H 2014 *Applied Physics Letters* **105** 092602
- [22] Scigaj M, Gázquez J, Varela M, Fontcuberta J, Herranz G and Sanchez F 2015 *Solid State Ionics* **281** 68
- [23] Delahaye J and Grenet T 2012 *Journal of Physics D: Applied Physics* **45** 315301
- [24] Nakagawa N, Hwang H Y and Muller D A 2006 *Nature Materials* **5** 204
- [25] Kalabukhov A, Gunnarsson R, Börjesson J, Olsson E, Claeson T and Winkler D 2007 *Physical Review B* **75** 121404
- [26] Siemons W, Koster G, Yamamoto H, Harrison W A, Lucovsky G, Geballe T H, Blank D H and Beasley M R 2007 *Physical Review Letters* **98** 196802
- [27] Herranz G, Basletić M, Bibes M, Carrétéro C, Tafrá E, Jacquet E, Bouzehouane K, Deranlot C, Hamzić A, Broto J M *et al.* 2007 *Physical Review Letters* **98** 216803
- [28] Cancellieri C, Reyren N, Gariglio S, Caviglia A, Triscone J M *et al.* 2010 *Europhysics Letters* **91** 17004
- [29] Herranz G, Sánchez F, Dix N, Scigaj M and Fontcuberta J 2012 *Scientific Reports* **2** 758
- [30] Breckenfeld E, Bronn N, Karthik J, Damodaran A, Lee S, Mason N and Martin L 2013 *Physical Review Letters* **110** 196804

- [31] Asmara T, Annadi A, Santoso I, Gogoi P, Kotlov A, Omer H, Motapothula M, Breese M, Rübhausen M, Venkatesan T *et al.* 2014 *Nature Communications* **5** 3663
- [32] Li C, Liu Z, Lü W, Wang X R, Annadi A, Huang Z, Zeng S, Venkatesan T *et al.* 2015 *Scientific Reports* **5** 13314
- [33] Gariglio S, Fête A and Triscone J M 2015 *Journal of Physics: Condensed Matter* **27** 283201
- [34] Scheiderer P, Pfaff F, Gabel J, Kamp M, Sing M and Claessen R 2015 *Physical Review B* **92** 195422
- [35] Thiel S, Hammerl G, Schmehl A, Schneider C and Mannhart J 2006 *Science* **313** 1942
- [36] Ahn C, Bhattacharya A, Di Ventra M, Eckstein J, Frisbie C D, Gershenson M, Goldman A, Inoue I, Mannhart J, Millis A J *et al.* 2006 *Reviews of Modern Physics* **78** 1185
- [37] Yoshida C, Tamura H, Yoshida A, Kataoka Y, Fujimaki N and Yokoyama N 1996 *Japanese Journal of Applied Physics* **35** 5691
- [38] Pallecchi I, Grassano G, Marr D, Pellegrino L, Putti M and Siri A S 2001 *Applied Physics Letters* **78** 2244
- [39] Ueno K, Inoue I, Akoh H, Kawasaki M, Tokura Y and Takagi H 2003 *Applied Physics Letters* **83** 1755
- [40] Inoue I 2004 Electrostatic tuning of oxide interfaces annual Report FY2003, Correlated Electron Research Center (CERC)
- [41] Shibuya K, Ohnishi T, Lippmaa M, Kawasaki M and Koinuma H 2004 *Applied Physics Letters* **85** 425
- [42] Shibuya K, Ohnishi T, Uozumi T, Sato T, Lippmaa M, Kawasaki M, Nakajima K, Chikyow T and Koinuma H 2006 *Applied Physics Letters* **88** 212116
- [43] Nakamura H, Takagi H, Inoue I H, Takahashi Y, Hasegawa T and Tokura Y 2006 *Applied Physics Letters* **89** 133504
- [44] Shibuya K, Ohnishi T, Sato T and Lippmaa M 2007 *Journal of Applied Physics* **102** 083713
- [45] Shibuya K, Ohnishi T, Uozumi T, Sato T, Nishio K and Lippmaa M 2008 *Applied Physics Letters* **92** 032109
- [46] Caviglia A, Gariglio S, Reyren N, Jaccard D, Schneider T, Gabay M, Thiel S, Hammerl G, Mannhart J and Triscone J M 2008 *Nature* **456** 624
- [47] Ueno K, Nakamura S, Shimotani H, Ohtomo A, Kimura N, Nojima T, Aoki H, Iwasa Y and Kawasaki M 2008 *Nature Materials* **7** 855
- [48] Bell C, Harashima S, Kozuka Y, Kim M, Kim B, Hikita Y and Hwang H 2009 *Physical Review Letters* **103** 226802
- [49] Cen C, Thiel S, Mannhart J and Levy J 2009 *Science* **323** 1026
- [50] Nishio K, Abe T, Takahashi R and Lippmaa M 2010 *Japanese Journal of Applied Physics* **49** 125701
- [51] Lee Y, Clement C, Hellerstedt J, Kinney J, Kinnischtzke L, Leng X, Snyder S D and Goldman A M 2011 *Phys. Rev. Lett.* **106**(13) 136809 URL <http://link.aps.org/doi/10.1103/PhysRevLett.106.136809>
- [52] Li M, Graf T, Schladt T D, Jiang X and Parkin S S P 2012 *Phys. Rev. Lett.* **109**(19) 196803 URL <http://link.aps.org/doi/10.1103/PhysRevLett.109.196803>
- [53] Förg B, Richter C and Mannhart J 2012 *Applied Physics Letters* **100** 053506
- [54] Christensen D, Trier F, Chen Y, Smith A, Nygård J and Pryds N 2013 *Applied Physics Letters* **102** 021602
- [55] Hosoda M, Bell C, Hikita Y and Hwang H Y 2013 *Applied Physics Letters* **102** 103507
- [56] Eyvazov A B, Inoue I H, Stoliar P, Rozenberg M J and Panagopoulos C 2013 *Scientific Reports* **3** 1038
- [57] Eerkes P D, van der Wiel W G and Hilgenkamp H 2013 *Applied Physics Letters* **103** 201603
- [58] Biscaras J, Hurand S, Feuillet-Palma C, Rastogi A, Budhani R, Reyren N, Lesne E, Lesueur J and Bergeal N 2014 *Scientific Reports* **4** 6788
- [59] Gallagher P, Lee M, Williams J R and Goldhaber-Gordon D 2014 *Nature Physics* **10** 748

- [60] Liu W, Gariglio S, Fête A, Li D, Boselli M, Stornaiuolo D and Triscone J M 2015 *Applied Physics Letters Materials* **3** 062805
- [61] Hurand S, Jouan A, Feuillet-Palma C, Singh G, Biscaras J, Lesne E, Reyren N, Barthélémy A, Bibes M, Villegas J E, Ulysse C, Lafosse X, Pannetier-Lecoeur M, Caprara S, Grilli M, Lesueur J and Bergeal N 2015 *Scientific Reports* **5** 12751
- [62] Schultz M and Klein L 2007 *Applied Physics Letters* **91** 151104
- [63] Gross H 2009 *In-situ study of emerging metallicity and memory effect on ion beam bombarded strontium titane surface* Ph.D. thesis The State University of New Jersey
- [64] Cordero F 2007 *Physical Review B* **76** 172106
- [65] Cuong D D, Lee B, Choi K M, Ahn H S, Han S and Lee J 2007 *Physical Review Letters* **98**(11) 115503
- [66] Neville R C, Hoeneisen B and Mead C A 1972 *Journal of Applied Physics* **43** 2124
- [67] Müller K A and Burkard H 1979 *Physical Review B* **19** 3593
- [68] Hemberger J, Nicklas M, Viana R, Lunkenheimer P, Loidl A and Böhmer R 1996 *Journal of Physics Condensed Matter* **8** 4673
- [69] Saifi M A and Cross L E 1970 *Physical Review B* **2** 677
- [70] Rössle M, Kim K W, Dubroka A, Marsik P, Wang C N, Jany R, Richter C, Mannhart J, Schneider C W, Frano A, Wochner P, Lu Y, Keimer B, Shukla D K, Stremper J and Bernhard C 2013 *Physical Review Letters* **110** 136805